OBSERVATION OF AN HYDRAULIC JUMP IN A FALLING SOAP FILM

by

Stanley FM Steers

Submitted to the University Honors College in partial fulfillment

of the requirements for the degree of

Bachelor of Philosophy

University of Pittsburgh

2010

UNIVERSITY OF PITTSBURGH

University Honors College

This thesis was presented

by

Stanley FM Steers

It was defended on

April 8, 2010

and approved by

Daniel Boyanovsky, Professor, Physics and Astronomy, University of Pittsburgh

Paul Shepard, Professor, Physics and Astronomy, University of Pittsburgh

Xiao-Lun Wu, Professor, Physics and Astronomy, University of Pittsburgh

Mahesh Bandi, Post-Doctoral Fellow, Harvard University

Thesis Advisor: Walter I Goldburg, Professor Emeritus, Physics and Astronomy, University of Pittsburgh

OBSERVATION OF AN HYDRAULIC JUMP IN A FALLING SOAP FILM

Stanley FM Steers, B. Phil.

University of Pittsburgh, 2010

For several decades, gravity-driven soap films have served as a convenient system in which to study two-dimensional turbulence due to the relatively small thickness (on the order of microns) when compared to the surface area of the film. This thesis presents evidence of an heretofore unobserved phenomenon in soap films: a sudden increase in the thickness of the film by approximately 200 to 300 percent, which occurs over a distance of only several centimeters in the vertical flow direction. Both velocity and thickness measurements confirm this transition in thickness as well as its dependence on the width of the soap film. In collaboration with theorists from the University of Illinois Urbana-Champaign, this thickness transition is explained as an hydraulic jump. The flow upstream and downstream is confirmed to be supercritical and subcritical, respectively, when compared to the propagation of elastic waves in the film as hydraulic jump theory would predict.

TABLE OF CONTENTS

LIST OF FIGURES

1.0 INTRODUCTION

1.1 BASICS OF FLUID DYANAMICS

1.1.1 The Navier-Stokes Equation

The fundamental dynamical equation for incompressible Newtonian fluid flows, such as those in water, is the Navier-Stokes equation (NSE),

$$\frac{\partial \mathbf{u}}{\partial t} + \mathbf{u} \cdot \nabla \mathbf{u} = -\frac{1}{\rho}\nabla p + \nu \nabla^2 \mathbf{u} + \frac{1}{\rho}\mathbf{F} \tag{1.1}$$

where $\mathbf{u}$ is the vector-valued velocity field, p is the scalar-valued pressure field, and ν is the kinematic viscosity, defined as the viscosity μ divided by the fluid density ρ. The notation $\mathbf{u} \cdot \nabla \mathbf{u}$ corresponds to $u_x \frac{\partial \mathbf{u}}{\partial x} + u_y \frac{\partial \mathbf{u}}{\partial y} + u_z \frac{\partial \mathbf{u}}{\partial z}$, which when added to $\frac{\partial \mathbf{u}}{\partial t}$ is known as the *substantive derivative*. $\mathbf{F}$ corresponds to *body forces*, which are forces acting on and within the fluid that do not arise from the dynamics of the fluid itself, such as gravity or the electromagnetic force (if the fluid carries a charge). In this form, the Navier-Stokes equation gives the acceleration at a point in the fluid, and when multiplied by ρ we have the force per unit volume of fluid. This formulation assumes that the fluid can be treated as a continuous medium that supports a velocity field and ignores the dynamics of particular molecules of

fluid. Conservation of mass requires that

$$\frac{\partial \rho}{\partial t} = -\nabla \cdot (\rho \mathbf{u}) \tag{1.2}$$

Since we are considering incompressible fluids (ρ is a constant), we are lead to a second equation:

$$\nabla \cdot \mathbf{u} = 0 \tag{1.3}$$

This equation, together with the Navier-Stokes equation and suitable boundary conditions, provides a closed set of equations that uniquely determine the velocity field $\mathbf{u}$. We shall assume the **stick boundary condition**, which dictates that the fluid next to a solid surface must have the same velocity as that surface.

The one left-hand term of the Navier-Stokes equation, $\mathbf{u} \cdot \nabla \mathbf{u}$, is called the *inertial* term. If a fluid particle is placed at a point of non-zero velcoity in the field x_0, the local velocity $\mathbf{u}(x_0, t)$ will carry it to a new location x_1 with corresponding velocity $\mathbf{u}(x_1)$, resulting in a change in the velocity of the particle to $\mathbf{u}(x_1, t)$. The intertial term corresponds to a differential of such a change in velocity. On the right hand side is the *viscous* term $\nu \nabla^2 \mathbf{u}$. The viscous term arises due to interactions between the molecules of the fluid and acts to oppose deformation of the fluid body. For a general fluid, the strain tensor (giving the deformation of the fluid in various directions) will have some relation to the stress tensor (giving the forces acting on surfaces of varying orientation within the fluid). Many everyday fluids exhibit a linear relationship between the stress tensor and the rate of strain tensor, and these are defined as *Newtonian* fluids. Water is an example of a Newtonian fluid, and we shall only encounter Newtonian fluids in this paper. When dealing with incompressible flows,

application of Eq. (1.3) further simplifies the relationship to only rely upon the Laplacian of the velocity [1],[2].

1.1.2 The Reynolds Number

Expressing the variables of Eq. (1.1) in dimensionless form (denoted by primes on the variables) yields

$$\frac{\partial \mathbf{u'}}{\partial t'} + \mathbf{u'} \cdot \nabla' \mathbf{u'} = -\nabla' p' + \frac{1}{\mathbf{Re}} \nabla'^2 \mathbf{u'} \tag{1.4}$$

where $\mathbf{Re} = \frac{UL}{\nu}$ is the **Reynolds number**, U being a characteristic velocity of the system and L a characteristic length [1]. Since all other quanities in this modified equation are dimensionless, two systems will have the same dynamical outcome provided that they have the same value for **Re**. An example of the application of the Reynolds number is a pipe, where U is the mean velocity in the pipe, L is the pipe radius, and ν is 0.01 cm^2/s, the kinematic viscosity of water. Doubling the radius of the pipe while halving the mean flow speed (by decreasing the pressure gradient across the pipe) will not change the value of **Re**, thereby preserving the form of Eq. (1.4) and yielding the same qualitative aspects for the flow. However, defining the Reynolds number for some systems is more complicated, especially for those systems which involve several different length and velocity scales. Yet the Reynolds number still gives some insight into such systems. Physical intuition can be gained by noting that the Reynolds number approximately gives the ratio of the inertial to the viscous term. Therefore, the Reynolds number gives an idea of the energy damping effects of viscosity versus the inertial energy of the fluid, and systems with similar energy balances should share broad qualitative features. Furthermore, we can expect more vigorous flow

behavior for higher values of **Re** due to the proportionally lesser effects of energy damping.

The Reynolds number may seem unnecessary since Eqs. (1.1) and (1.3) provide all the information necessary to solve for the velocity field. However, the Navier Stokes equation [Eq.(1.1)] is non-linear in nature, the non-linearity arising from $\mathbf{u} \cdot \nabla \mathbf{u}$. For the vast majority of non-linear differential equations general solutions are unknown, and unlike linear equations which obey the superposition principle, general solutions cannot be constructed as linear combinations of specific solutions [3]. For physical applications, this difficulty is often surmounted by settling for qualitative information about solutions, imposing some assumptions that simplify the equations, or using numerical techniques. One standard technique involves finding a domain on which the solution of the non-linear equation is well approximated by the solution to a simpler linear equation. The non-linearity of the Navier-Stokes equation generally only admits linearization by ignoring the inertial term (thereby assuming **Re** is much less than one), and the resulting equation is known as the *creeping motion* equation [2].

However, the bulk of physically interesting fluid flows cannot be modelled without the non-linear inertial term. Non-linear partial differential equations such as the NSE often have solutions with features such as chaos, shocks (discontinuities in the solution, sometimes representing two formally different solutions on either side of the discontinutiy,) and special waves known as *solitons*, features that have no analogues among the solutions of linear differential equations [3]. Indeed, the entire field of turbulent fluid flows is intimately connected with non-linearities in the governing equations [4]. Ignoring the inertial term does not make the job of airline pilots any easier. This forces fluid dynamicists to rely upon the qualitative information mentioned earlier or computational methods. However, computational methods

have only recently become practicable, and for well over a century much progress in fluid dynamics has come from direct observation of fluid systems under a wide variety of parameters. As such, fluid dynamics is widely characterized by multiple clases of possible flow patterns, grouped by the general set-up of the system. Examples of such classes are Couette flow, which involves a fluid confined between rotating cylinders, stratified flow, which invloves several fluids of different densities in the same system, and convective flow, where externally imposed temperature differences lead to gradations in density. One important class of flows, free surface flows, will be discussed in further detail in Sec. 1.3.

1.2 DIMENSIONALITY OF FLUID FLOWS

The Navier-Stokes equation is equally valid in one, two, and three dimensions, and should a fluid exist only in two dimensions the corresponding velocity field would still solve the NSE. Everyday systems are not truly constrained to a two-dimensional (2D) world, but a fluid system could be effectively 2D. In some cases, this will hold if the fluid is 3D but only flows in parallel layers such that the velocity perpendicular to these layers, call it u_z, is zero. This condition will approximately hold if the boundaries of the system in the z direction are so distant from the measurement point that the fluid could be considered to extend infinitely in this direction [2]. In other cases the extent of the system in one of the three dimensions is negligible compared to the extent in the other two dimensions, and although the fluid may have a non-zero velocity component in this direction such motion will, like the length scale in this direction, be small enough to be ignored when compared to the velocity componenets in the other directions. Such considerations have resultecd in

2D models of large-scale atmospheric phenomena, and these models constitute some of the more compelling reasons for studying the particular properties of 2D flows [5].

At first glance it may appear that treating a system as two-dimensional is merely a simplification, but this is not necessarily the case. Not only do 2D flows exhibit a rich set of complex behaviors like their 3D counterparts, but the dimensionality of the system actually alters the qualitative aspects of the flow. One major difference involves the transfer of energy between different *length scales* in turbulent flows. Formally, we define a length scale by the corresponding spatial Fourier component k of the velocity fluctuations [4]. Informally, a length scale can be understood by thinking of a single eddy within a fluid. With the size of the eddy is associated a particular length scale, and the kinetic energy of the eddy is also connected with this length. Should the flow contain two eddies with one eddy twice as large as the other, we would say that some part of the energy of the flow is at the length scale of the larger eddy, and some of the energy is at the length scale of the smaller eddy. Should the larger eddy break apart into two smaller eddies, we would say that energy has been transferred between length scales. This image of a well-defined eddy naturally connects with the notion of a spatial Fourier component. If we were to draw a line in the plane of the eddy passing through its center and take the velocity component perpendicular to this line at each spatial point, on one side of the line the fluid would be moving in the opposite direction as the fluid on the other side of the line. Plotting the velocity as a function of spatial position on either side of this bisecting line would roughly give a sine curve. Should several vortices come together, the respective motions of the several eddies may destroy the regular eddy structure. However, the spatial Fourier transform will still reveal contributions from the length scales that characterized the original set of eddies.

The velocity fluctuations associated with turbulent flow can also be envisioned as the interaction between many eddies of different sizes. In 3D turbulent flows, larger eddies break apart into smaller eddies, causing energy to move from large to small length scales in what is known as the *energy cascade* [4]. However, in 2D trubulent flows smaller eddies join together to form larger eddies and thereby transfer energy from small to large length scales in what is known as the *inverse energy cascade*. This markedly different behavior makes 2D flows of at least theoretical interest. Furthermore, this tendency for vortices to coalesce in 2D turbulence has direct consequences for the previously mentioned atmospheric models, explaining the tendency for small rotating storm cells to come together to from larger storm cells.

1.3 FREE SURFACE FLOWS

One of the several different classes of fluid flows mentioned in Sec. 1.1, a *free surface flow* is a flow such that the fluid is confined to move within some conduit or container such as a trough, half-pipe or a river bed whereby one edge of the fluid, known as the *free surface*, is subject to atmospheric pressure. Since the free surface is subject to atmospheric pressure and gravity, this surface is free (hence the name) to alter its shape, unlike the situation where the surface must conform to a solid surface such as the top half of a pipe. This freedom allows a number of different flow features related to changes in the free surface shape. These changes are usually expressed in terms of the *depth of flow* y, which gives the vertical distance from the free surface to the channel bottom. Although systems where the two dimensions that form the area of the free surface can be of the same order, such as in

a circular lake or a cubical container of water, many interesting flows will have a dominant direction of bulk flow, such as the downstream direction in a river. Free surface flows are often categorized by how the depth of flow changes with respect to time and distance [6]. If the depth of flow at a given point changes in time, then the flow is *unsteady*, while the flow is *steady* if it does not change with time. If the depth of flow changes with respect to the downstream direction, it is labelled as *varied*, and naturally as *unvaried* if it does not. Varied flow can further be broken down into *gradual* and *rapid* varieties, depending on how quickly the depth changes with the downstream direction. Naturally, an increase in the

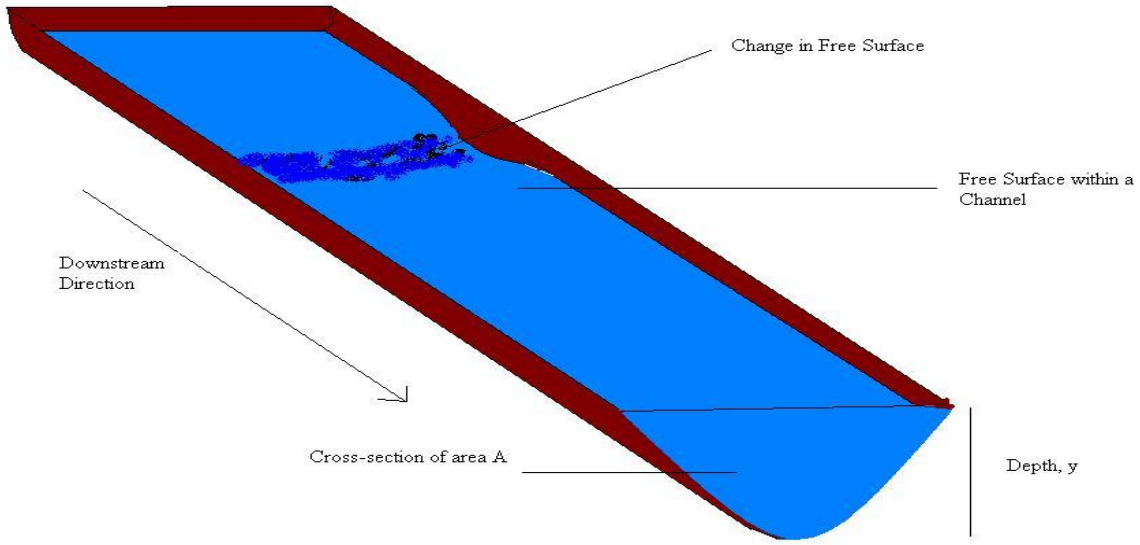

Figure 1.1: A typical free surface flow in a channel.

depth of flow will be opposed by gravity, which will play an important role in determining the specific shape of the free surface. Thus we can characterize free surface flows by a second

dimensionless parameter akin to the Reynolds number. Known as the *Froude* number, this quantity gives the approximate ratio of the inertial term to the body force term due to gravity [6]. Dimensional arguments (ignoring viscous term in the NSE) yield

$$\mathbf{Fr} = \frac{U}{\sqrt{gy}},$$

where g is the acceleration due to gravity and y some characteristic length scale. Typically, the characteristic velocity U is taken as the average velocity in the downstream direction, while the characteristic length is taken as the *hydraulic depth*, which is equal to the cross-sectional area perpendicular to the downstream direction divided by the width of the free surface. Flows where $\mathbf{Fr} > 1$ are known as *supercritical* flows, while if $\mathbf{Fr} < 1$, the flow is *subcritical*. As can be readily guessed from the other names, if $\mathbf{Fr} = 1$, then the flow is *critical*. Depending on the value of the Reynolds number, both subcritical and supercritical flows can be laminar or turbulent. Further information can be extracted from the Froude number by noting that $\mathbf{Fr} = 1$ when $U = \sqrt{gy}$, which is also the velocity of small gravity waves should the fluid be shallow [6]. Thus, in subcritical flow it is possible for gravity waves to travel upstream against the prevailing current, while in supercritical flow it is not.

The concepts of supercritical and subcritical flow are not limited to shallow water waves, but are applicable to any free surface flows so long as there is a force that opposes deformation of the free surface and hence, where waves can propagate. Such a force might be the elastic force of surface tension. Even if the surface were not perpendicular to the force of gravity, waves could still propagate along the surface due to the restoring force associated with surface tension. These waves will have a characteristic velocity depending on the medium, and thus the flow will be supercritical if the flow velocity is greater than this propagation velocity, and

subcritical if the flow velocity is less. The Froude number concept still applies, but now gives the ratio of the velocity to the velocity of surface wave propagation. The difference between supercritical and subcritical flows is highlighted by the propagation of surface disturbances caused by an object placed in the flow. In a supercritical flow, surface disturbances caused by the object cannot propagate against the mean flow direction since this velocity is greater than the characteristic velocity of the waves. These waves will only propagate downstream, and as they do so subsequent waves will overlap to form a shock front that flares outward in the wake of the object. The situation is entirely analogous to that of supersonic flight, where sound waves can overlap to form a sonic boom since the relative velocity between the aircraft and the air is greater than the speed of sound. Since subcritical flows have a velocity less than that of the propagation velocity for shallow water waves, no shock front forms, only a regular wake for the object.

Taking some point B in the flow, the energy per unit weight of fluid passing through that point is comprised of the kinetic energy of the fluid passing through that point, the gravitational potential energy of that point (with respect to some reference height) and the weight of the column of fluid above the point and below the free surface. This translates into equation form as

$$\frac{E}{\rho g} = z_B + d_B \cos\theta + \frac{V_B^2}{2g} \tag{1.5}$$

where z_B is the height above the potential energy reference point, d_B is the depth of the point from the surface, θ is the angle of the bottom of the channel makes with the horizontal, and V_B is the velocity of the fluid at B. Obviously, multiplying through by ρg would give more familiar energy terms such as $\rho g h$, while Eq. (1.5) has units of length, since it is energy per unit weight of fluid. Integrating over a cross-sectional area perpendicular to the mean flow

direction yields the total energy per unit weight of fluid for the entire cross-section, provided the velcoity varies slowly over the cross-sectional area.

The Froude number can also be related to energy principles. When the potential energy reference point is taken as the bottom of the channel ($z = 0$), the energy per unit weight of fluid is known as the *specific energy*. Conservation of mass requires that the flux Q through a channel cross-section must equal the average velocity $\bar{V}$ times the cross-sectional area A. Substituting for $\bar{V}$ in the specific energy yields

$$\frac{E}{\rho g} = y + \frac{Q^2}{2gA(y)^2} \tag{1.6}$$

where we have taken $\theta \approx 0$ as well as making the dependence of the area on the depth of flow y explicit. A graph of specific energy versus depth is shown in Fig. 1.2. Notably, the depth of flow as a function of specific energy is not single-valued. Rather, there are two possible channel flows for any particular specific energy, one of greater depth and smaller mean flow velocity, and one of lesser depth and greater mean flow velocity. However, there is a single point on the specific energy curve such that these two *alternate* depths, as they are called, become one, the *critical depth*, y_c. Through differentiating Eq. (1.6) with respect to y [6], we can find this point by solving for the minimum of the specific energy as a function of height,

$$\frac{1}{\rho g}\frac{dE}{dy} = 1 - \frac{Q^2}{gA^3}\frac{dA}{dy} = 1 - \frac{\bar{V}^2}{gA}\frac{dA}{dy} = 1 - \frac{\bar{V}^2 T}{gA} = 1 - \frac{\bar{V}^2}{gD} = 0 \Rightarrow \frac{\bar{V}^2}{2g} = \frac{D}{2} \tag{1.7}$$

where we have used $\frac{dA}{dy} = T$, where T is the width of the free surface, and we have noted that the hydraulic depth D is $\frac{A}{T}$. The last implication can be rewritten $\frac{\bar{V}}{\sqrt{gD}} = 1$, which is precisely the requirement for critical flow. This also reveals that for points on the specific energy curve above the critical depth the flow is subcritical, while for points corresponding to

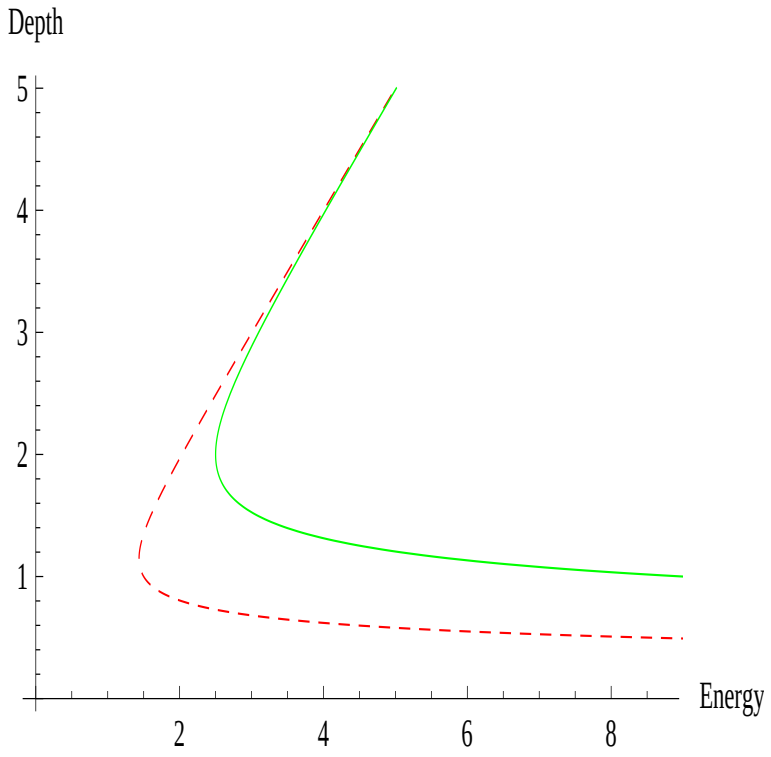

Figure 1.2: Plot in dimensionless units of depth versus specific energy for a higher (solid green line) and lower (dashed red) value of the flux, Q.

depths less than y_c, the flow is supercritical. It is possible for flows to change from subcritical to supercritical regimes and vice versa by changing their depth, often resulting in interesting non-linear behavior.

1.3.1 The Hydraulic Jump

One of the most readily observed non-linear phenomena in free surface flows is the *hydraulic jump*. A form of the hydraulic jump occurs in the everyday setting of the kitchen sink. After the initial impact of the stream from the faucet, the water moves out radially at some constant *initial* depth until a distance r_j, at which point the depth rapidly increases over a short distance to the *sequent* depth, which is then maintained as the fluid continues to move radially outward (Fig. 1.3). This is known as the *circular* hydraulic jump. The hydraulic jump also occurs in open channels, where the sudden transition from a shallow depth to a greater downstream depth is known as the *linear* hydraulic jump.

The detailed structures of both the linear and circular hydraulic jump are still not fully understood, although the location at which each type of jump occurs can now be modelled fairly well. An early approach to the linear hydraulic jump is due to Lord Rayleigh, who ignored viscosity and focused on momentum conservation across the jump, which he took to take place across an infinitessimal downstream direction as a shock (thereby justifying the assumption that friction from the channel was negligible) [7],[8]. To this end, let us take note of the forces upon a cross-section of fluid as it travels downstream, namely the force $P_1 - P_2$ due to the pressure differential , the force of gravity $W \sin\theta$, where W is the weight of the fluid in the cross-section, and the frictional forces at the boundary of the channel, F_f [6]. Newton's second law equates this with the time change of momentum, which can be

Figure 1.3: A circular hydraulic jump in the author's kitchen sink. Author's own photograph.

written

$$P_1 - P_2 + W\sin\theta + F_f = \frac{Qw}{g}(\bar{V_2} - \bar{V_2}) \tag{1.8}$$

where w is the unit weight of the fluid. Following the lead of Lord Rayleigh [7], we assume the frictional forces are negligible over the short distance in which the jump occurs. Further simplifying, we take the channel as horizontal and as being rectangular with a constant width. Conservation of momentum implies $y_1\bar{V_1} = y_2\bar{V_2}$ where y_1,y_2 are the initial and sequent depths, respectively, while the force due to the pressure differential can be stated so that the momentum flux is:

$$y_1\bar{V_1}(\bar{V_1} - \bar{V_2}) = \frac{1}{2}g(y_2^2 - y_1^2) \tag{1.9}$$

This equation, when combined with $y_1\bar{V_1} = y_2\bar{V_2}$, can be used to solve for the initial and final velocity should the initial and sequent depths (y_1,y_2) be known, and thus (omitting some of the algebra)[7],

$$\bar{V_1}^2 = \frac{1}{2}g(y_1 + y_2)\frac{y_2}{y_1} \text{ and } \bar{V_2}^2 = \frac{1}{2}g(y_1 + y_2)\frac{y_1}{y_2} \tag{1.10}$$

while noting the definition of $\mathbf{Fr} = \frac{\bar{V_1}}{\sqrt{gy_1}}$ for the *incoming* flow provides a different arrangement of the variables [6]

$$\begin{aligned}
&(\frac{y_2}{y_1})^3 - (2\mathbf{Fr}^2 + 1)\frac{y_2}{y_1} + 2\mathbf{Fr}^2 = 0 \\
&\Rightarrow (\frac{y_2}{y_1})^2 + \frac{y_2}{y_1} - 2\mathbf{Fr}^2 = 0 \\
&\Rightarrow \frac{y_2}{y_1} = \frac{1}{2}(\sqrt{1 + 8\mathbf{Fr}^2} - 1)
\end{aligned} \tag{1.11}$$

As the fluid travels down the channel, frictional forces remove energy and cause the fluid to slow, and to become deeper so as to satisfy the conservation of mass. If the downstream depth achieves y_2, then the transition to a greater downstream depth will take the form

of a jump at the location where the depth and velocity of the incoming flow satisfy Eq. (1.11). This transition in the depth corresponds to the flow changing from a supercritical state to a subcritical state, which is why the Froude number comes into play. As the flow loses energy, the dynamical conditions become such that the flow can switch between the two branches of the specific energy curve (Fig. 1.2). Such considerations often lead hyraulic engineers to alter the shape of the channel downstream of some point at which they desire a hydraulic jump to occur, thereby setting y_2 so that Eq. (1.11) will be satisfied for some existing flow pattern [6]. The benefit of this action is to reduce the energy content of the flow, which may be desirable in a number of situations, such as when a less energetic flow is required to prevent erosion of a natural channel. Although for momentum conservation it was assumed that *external* frictional forces were negligible, a standard hydraulic jump will still have considerable dissipation of energy due to the *internal* effects of viscosity, which is why conservation of momentum rather than conservation of specific energy was used to derive the previous equations. Again, it was Lord Rayleigh [7] who, by comparing the sum of the kinetic and potential energy of the flow before and after the jump, showed that the loss in energy is

$$\delta E = y_1 \bar{V}_1 \frac{(y_2 - y_1)^3}{4 y_1 y_2} \tag{1.12}$$

Of course, should the channel have a more complicated shape than the rectangular one presented here, the previously derived relationships may not precisely hold, although for a horizontal channel of constant cross-section the terms in Eq. (1.8) will have the form

$$F = \frac{Q^2}{gA} + \bar{z}A,$$

where $\bar{z}$ is the centroid of the cross-section. Should the channel not have a constant cross-section for more than a small section of the channel, using conservation of momentum to

calculate the aspects of the jump becomes problematic as pressure distributions and total momentum flux become more specific functions of position. In addition, this treatment has taken the hydraulic jump as a transition in depth that occurs over an infinitessimal distance. This would imply that the fluid depth has a discontinuity at the point of the jump, which both experiments and common sense do not support. However, even if the assumption of an infinitessimal distance for the jump was relaxed, the theory still does not touch upon the different types of internal structure that are observed in acutal jumps. The hydraulic jump naturally involves a continuous change in the depth of flow over a finite distance, and the particular structure of this change can vary depending upon the Froude number of the incoming flow and the particular channel shape. For instance, the free surface during the jump could exhibit undulations in an *undulating* jump, the transition region might have a large degree of turbulence, or an irregular burst of fluid could circulate from the bottom of the channel to the free surface of the jump, creating strong waves that then travel great distances down the channel [6]. One technique [9] used to further analyze the hydraulic jump treats the jump as a combination of discontinuous waves travelling in the channel, which helps to explain some of the waves associated with jumps such as the undulating jump. This technique gives a reasonable approximation only for a small range of hydraulic jumps, and still invloves discontinuities in the underlying equations. The continued presence of such discontinuties, or shocks as noted in Sec. (1.1.1), highlights the non-linear nature of the hydraulic jump that was obfuscated by the ease of the previous momentum conservation argument. Indeed, Lord Rayleigh himself viewed the hydraulic jump as a shock in the shallow water equations [8], an approximation to the NSE and the traditional continuity equation $\frac{\partial \mathbf{u}}{\partial t} = -g\nabla h$ and $\frac{\partial \ddot{h}}{\partial t} + \nabla \cdot (\mathbf{u}\ddot{h})$, where h is the height of the free surface with respect to some

reference point and $\ddot{h}$ is the height of the channel bottom above the same reference plane [10]. If the channel bottom is flat, then we can take $\ddot{h} = h$.

Unlike the linear hydraulic jump, the circular hydraulic does not yield any secrets to an inviscid (or ignoring viscosity) analysis. The more successful approaches such as that by Bohr et. al [8] have made use of an approximation scheme that includes viscosity known as *boundary layer theory*. An extremely rich subfield of fluid dynamics first proposed by Prandtl [11], we will only touch upon a few of the basics of boundary layer theory here. Boundary layer theory simplifies the NSE by assuming that Euler's equation (which is Eq. (1.1)ignoring viscosity) will hold for the bulk of a fluid with high Reynolds number but that viscosity will become more prominent in thin regions near the fluid boundaries, where the fluid velocity is necessarily smaller so as to satisfy the stick boundary condition. These thin regions near the boundaries of the fluid are intuitively the *boundary layers* for which the theory is named. Furthermore, the velocity in the boundary layer is taken to be mostly tangential to the boundary, the magnitude of which changes rapidly as the distance to the boundary increases. Comparing the order of magnitude of various terms in the full NSE both in the boundary layer and in the bulk flow allow the elimination and substituion of certain terms.

As an example, take the boundary layer equations for a steady boundary layer on a flat surface, with x the direction and u the velocity component tangential to the wall, y and v the similar variables normal to the surface, and u_0 the bulk flow velocity which is only a function of x [2]:

$$u\frac{\partial u}{\partial x} + v\frac{\partial u}{\partial y} = u_0\frac{du_0}{dx} + \nu\frac{\partial^2 u}{\partial y^2} \tag{1.13}$$

$$\frac{\partial u}{\partial x} + \frac{\partial v}{\partial y} = 0 \tag{1.14}$$

The assumptions for the problem allowed the action of viscosity due to $\frac{\partial^2 u}{\partial y^2}$ to be ignored, and the insignificance of pressure differences across the boundary layer compared to the pressure gradient in the x direction allowed us to substitute the inertial term for flow in the bulk for the pressure gradient in the boundary layer. These simplifications allow us to solve for the bulk velocity independently of the stick boundary condition and then use this solution to find the particular form of the velocity near a boundary which does satisfy the stick boundary condition. Although boundary layer theory was first derived using scale arguments, this theory can be viewed as the first-order theory corresponding to a perturbative expansion of solutions to the NSE [11]. However, such depth of analysis is not required here.

Boundary layers are very important for the overall flow pattern, often giving rise to the peculiar aspects of fluid dynamics. Wakes are a result of boundary layers. The phenomenon of boundary layer separation is particularly pertinent to our current discussion, for it is what led Bohr et. al [8] to use boundary layer approximation techniques for the circular hydraulic jump. In boundary layer separation, the boundary layer is no longer confined to a small region near the boundary but becomes detached for some reason such as in the wake of an object where eddies can form, leading to sections of flow near the boundary that move in the opposite direction to the surrounding fluid. Similarly, a region of fluid near the bottom of the sink moving opposite to the mean flow direction has been observed in the circular hydraulic jump. Combining this with the fact that the flow in the hydraulic jump is generally in the tangential direction to the lower constraining surface suggests using the boundary layer equations in place of the traditional momentum-flux equation approach of Lord Rayleigh.

Bohr then took the boundary layer equations and integrated them over the depth at any given value of r, the distance from the inital impact point of the stream from the faucet and

divided by the depth. To perform this integration, the velocity as a function of depth was taken to be a third order polynomial in the depth (with suitable coefficients to be fitted to experiment). This procedure gave the average momentum passing by any radial point, which could then be used to find the surface profile in the jump region. This gave decent agreement with experimental results both in the general profile of the jump and the radial position r_j at which it would occur. Furthermore, nothing about Bohr's theory limits it to the circular hydraulic jump; it can just as well be applied to the linear hydraulic jump. Indeed, Bohr was able to show through an analysis of the propagation of waves in his model that the notions of supercritical and subcritical flow from traditional approaches was consistent with his approach.

2.0 EXPERIMENT

2.1 SOAP FILMS

As noted in Sec. 1.2, 2D flows are of considerable interest not only as models of 3D systems such as the atmosphere but as sources of qualitative behavior different from that found in 3D flows. One way of studying 2D flows is to use soap films. Although soap films have been an object of experimental curiosity for over a century, it was not until the work of Couder [12] that soap films were investigated as fluid dynamical systems. Surfactants like every day dish soap are generally constituted by molecules with two distinct parts: a hydrophilic polar head which is attracted to the polar water molecule, and some group of hydrocarbons, usually strung out in a tail, that is hydrophobic. These competing properties give soap its utility as a cleaner, allowing it to attract both water and hydrophobic chemicals such as oils. The hydrophobic/hydrophilic duality also allows soap solutions to create films. In a soap/water solution, it is energetically favorable for soap molecules to deposit themselves near a free surface, where their hydrophobic tails can orient away from the water moelcues. The molecules will therefore move to the fluid surface until their is thermodynamic equilibrium between molecules at the surface and those in the bulk. Such positioning creates a thin, uniform structure at any free surface as soap molecules line up next to each other with tails

pointing out and heads facing into the solution.

The surface tension associated with this arrangement makes films stable; the segregation of surfactant and water molecules promotes the initial formation of films with larger surface area (compared to pure water, which would naturally bead), while the restoring forces of surface tension promote a greater degree of elasticity, allowing the topology of the film some freedom to deform without leading individual regions of fluid to separate from the bulk and form small spheres. The elastic force associated with the surface tension also allows waves to propagate along the surface of the film. It should be noted that there are two regimes of elastic force for the soap film. If the characteristic time of the deformation is much smaller than the time it takes soap molecules to diffuse into areas of lower concentration, (so that soap molecules do not have time to diffuse out of the bulk of the fluid,) then the elastic force is that of the *Marangoni* regime. If the deformation occurs on a longer time scale and particles do have time to diffuse onto the surface, the surface tension will change accordingly and the film is in the *Gibbs* regime. In this experiment, the film will be in the Marangoni regime.

With a thickness on the order of a few microns or less, the soap film made possible by surface tension will be very thin compared to the two dimenions that make up the surface area of the film. Indeed, films can be produced that are several centimeters wide and several meters long [13]. Furthermore, the film itself can flow as a fluid while maintaining the overall shape of the film. This makes a soap film a good candidate for investigating 2D flows. It was one such investigation, namely that of finding the coefficient relating the energy loss in the film due to friction to the physical dimensions of the soap film (known as the friction factor) that led to unexpected observations, which are presented here.

2.2 APPARATUS

The apparatus for this experiment follows in the tradition of Couder [12] and later Rutgers et. al. [13]. In initial experiments, a water/soap solution that is 1.5 ± 0.3% Dawn Non-Ultra dish detergent by volume is allowed to flow under the force of gravity from an elevated reservoir down two nylon fishing lines, marked WR and WL in Fig. 2.1, reproduced from [5]. These lines are held taught by a suspended weight (W), and the solution drains into a bottom reservoir (RB)to be pumped back up to the top reservoir by the pump (P). In this way a continuous flow can be maintained. When the wires are drawn apart horizontally by secondary draw lines, a soap film forms between the wires with a thickness $h \approx 10$ microns for the average film. As mentioned in Sec. 2.1, this makes the soap film essentially two-dimensional. However, the thickness might still be a function of position, labelled (x, z) in Fig. 2.1, with positive x in the downward vertical direction from the nozzle. Measurements support the thickness being roughly constant in z for any value of vertical position x, we write $h = h(x)$. In addition, the vertical velocity u approximately will be independent of z, since the velocity will quickly approach some mean value $u(x)$ for small displacements from the wires in the z direction. When combined with an assumption of incompressibility, these approximations provide that, for a constant flux of fluid q per unit width, $q = h(x)u(x)$ will hold.

Initial observations were made with a soap film with a total length of 150 cm and a bottom section that tapered over the last 10 cm to the weight (unlike that shown in Fig. 2.2); it was found that whether the film tapered or did not taper before attaching to the weight made a negligible impact on our observations, and no distinction will be made between the

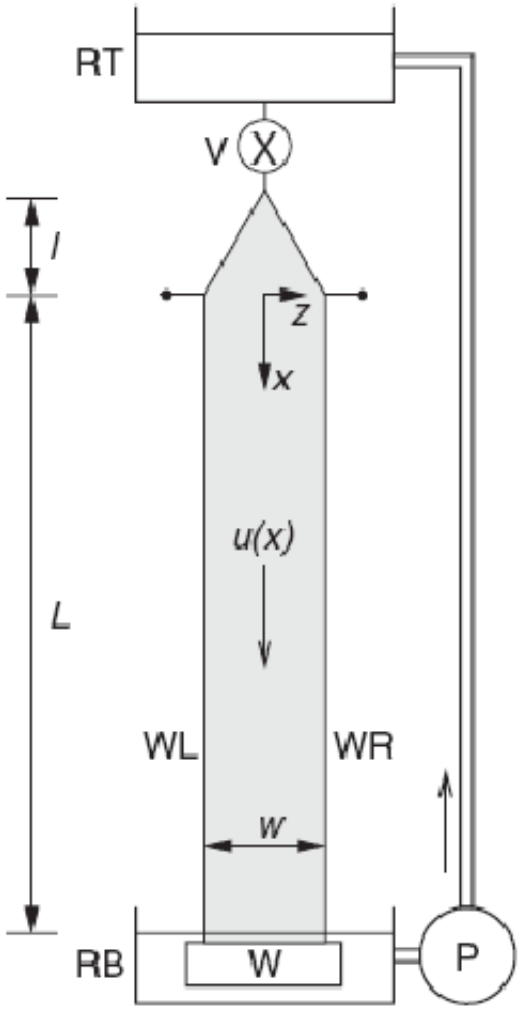

Figure 2.1: The apparatus for producing a stable soap film used in this experiment. The film has a thickness h (not shown) in a dimension perpendicular to the page and measured from one of the two faces at $x = 0$.

initial tapered set-up and later modifications to a non-tapered set-up. However, the ultimate length of the film did play a role in the experiment, and the length from the first set of draw lines to the weight (marked as L on the figure) ranged from 105.0 cm to 150.5 cm, while the length from the nozzle to the first draw lines (l on the figure) remained constant at 23.5 cm. The width of the film was an adjustable parameter and was typically in the range 1.00 cm to 5.10 cm.

2.3 EXPERIMENTAL TECHNIQUES

Several experimental techniques were used to investigate various properties of the soap film such as vertical velocity as a function of time and position $u(x,t)$, as well as the film thickness $h(x,z)$. Before describing our empirical results, we shall take a brief moment to explain the fundamentals of these measurement techniques.

2.3.1 Laser Doppler Velocimetry

Laser Doppler velocimetry (LDV) is a standard and very powerful technique for measuring fluid velocities. LDV converges two coherent light beams at a fixed angle of intersection onto a small volume of the fluid. Due to the relative angle of the two beams, an interference pattern is formed. Optical equipment then detects light scattered by small particles seeded into the fluid as they pass through this interference pattern. The envelope frequency of the scattered light will change with the velocity of the particle, and by comparing the expected frequency with the detected scattering frequency, the velocity can be determined [13]. LDV has the specific advantage that no physical object need be placed in the fluid flow to obtain

a velocity measurement, unlike the older technique of hot-wire anemometry, which required that a resistor be placed in the fluid flow so as to measure the rate of cooling of the resistor.

For this experiment, a commercial LDV system produced by TSI, Inc., was used in connection with an Innova-90 Argon/Krypton laser as well as the FlowSizer software from TSI. The particles used were polystyrene spheres, ranging from 0.10(2) microns in diameter to 4(1) microns in diameter. Although smaller sized particles with lesser variation in diameter were used in early experiments, it was found that more coarsely grained particles gave comparable scattering intensities and velocity measurements while reducing overall expenses. Not only could the average velocity over an extended period (possibly hours, although for our experiment it was generally 30 seconds) be measured with this instrumentation, but the velocity could be measured several thousand times per second, allowing a nearly instantaneous record of the velocity through time. This record could then be processed using a standard Fast Fourier Transform (FFT) program such as that found in MatLab to determine the power spectrum of the velocity or of the velocity squared. The power spectrum gives the strength of each Fourier component in the form of the modulus squared of the coefficient of the Fourier component.

2.3.2 Interference Photography

Just as glass slides can form an interference pattern when separated by a small distance, the two surfaces of the soap film will each reflect light and, should this light be monochromatic, very clear interference fringes will be observed that correspond to variations in the thickness. The closer the frignes, the greater the change in thickness in the direction perpendicular to the fringe contours. In this experiment, a sodium lamp was used to provide the

monochromatic light source. Initially, these fringes were photographed using a fast camera manufactured by Phantom 5, capable of taking over 1000 frames per second. However, such small time scales proved unnecessary to resolve the fringes, and a Canon S90 digital camera was used for the latter part of the experiment.

2.3.3 Fluorescein Dye Flourescence

The relative thickness of the film for various values of x was also ascertained through the use of Fluorescein, a common commercial dye that emits green light. After being added to the soap film, the dye initially was fluoresced using a 514 nm laser source such that the spot illuminated by the laser was of constant cross-sectional area, no matter what point on the soap film was illuminated. The intensity of the fluorescent light emitted by the point of illumination would only change if the thickness of the film changed, thereby changing the total flourescent volume. The intensity was measured by collecting a fixed portion of the light through a green-light filter into an avalanche photodiode. Although the method was too crude to give a quantified thickness value, it did provide the means to determine the ratio of the thickness measurements taken at two x values. Later measurements focused incoherent blue light onto the film so as to take advantage of the absorption peak of Fluorescein in the blue regime.

2.4 OBSERVATIONS

2.4.1 Velocity Profile

Initial observations of the vertical component of the velocity as a function of vertical position were made in connection with the investigation of the friction factor mentioned in Sec. 2.1. An example of these measurements for one of the longer films used, 175(1) cm, can be found in Figs. 2.2 and 2.3. The most immediate and striking feature of these graphs is the sudden drop in velocity that occurs over the space of approximately 25 cm. Before the precipitous drop in velocity, the velocity steadily increases. This behavior is expected since the fluid is falling under the force of gravity, and just like a a parachutist, we anticipate that the fluid will accelerate until the effects of air friction totally oppose further acceleration. However, rather than attaining and maintaining a maximum velocity, the fluid velocity decreases by nearly an order of magnitude before settling into a comparatively flat regime near the bottom of the film. In addition, note the larger error bars in the spatial region characterized by the decrease in velocity. This denotes greater fluctuations of the velocity about the recorded mean (the error bars in general probably arise due to fluctuations in the flux into the film, interactions with air currents, and small deviations of the system from steady state flow). Figure 2.2, which shows data for soap films with different values of qw, clearly shows that the position of the anomalous effect is dependent upon the flux, while Fig. 2.3, which now keeps qw constant but changes the width of the film, suggests the effect is independent of the width.

In collaboration with Gioia, Chakraborty, and Tran at the University of Illinois Urbana-Champaign, further velocity measurements were taken by Tran for various lengths of the film.

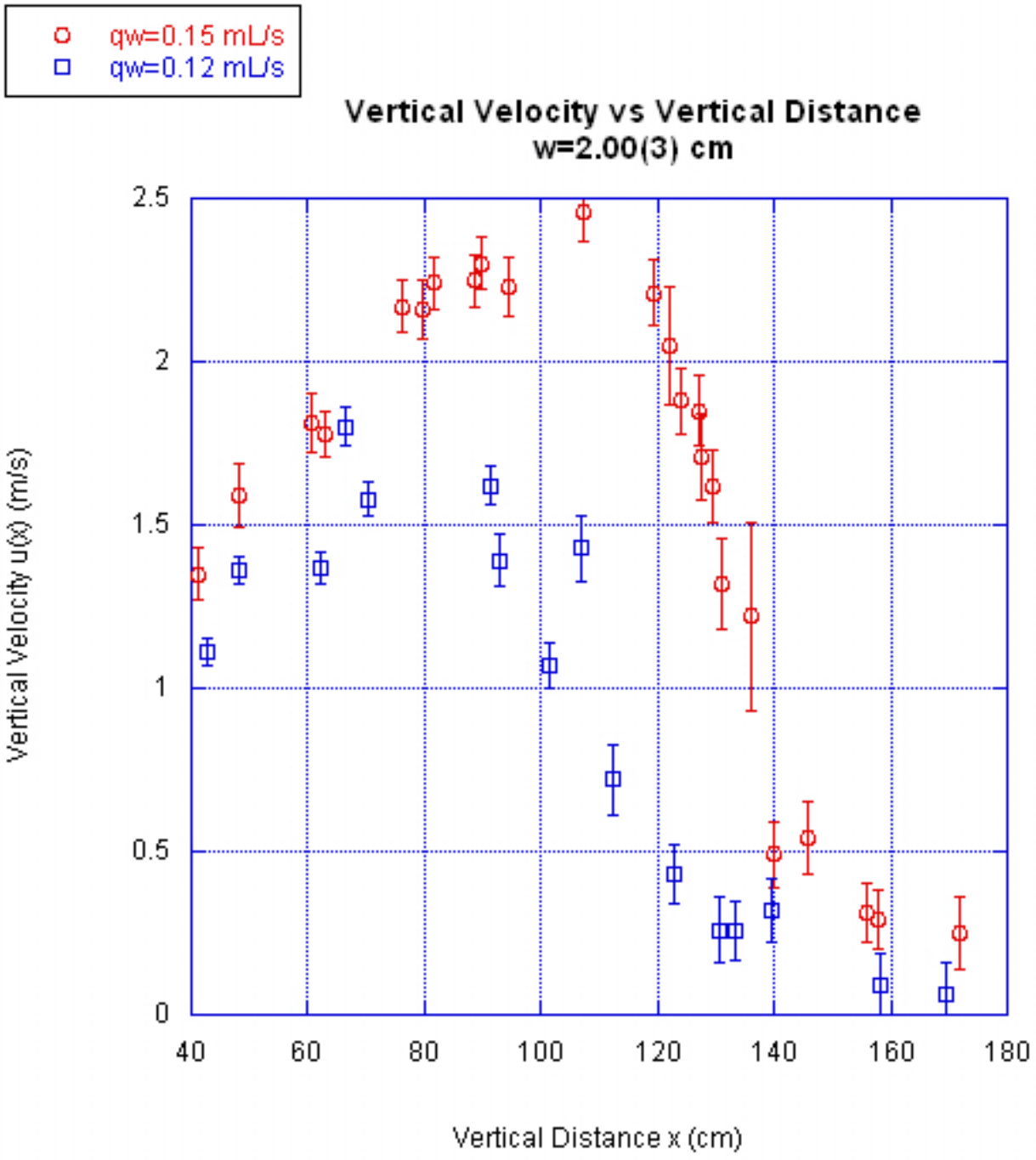

Figure 2.2: The velocity profile of a soap film of 2.00 cm width for two different qw values: qw=0.15 mL/s and qw=0.12 mL/s.

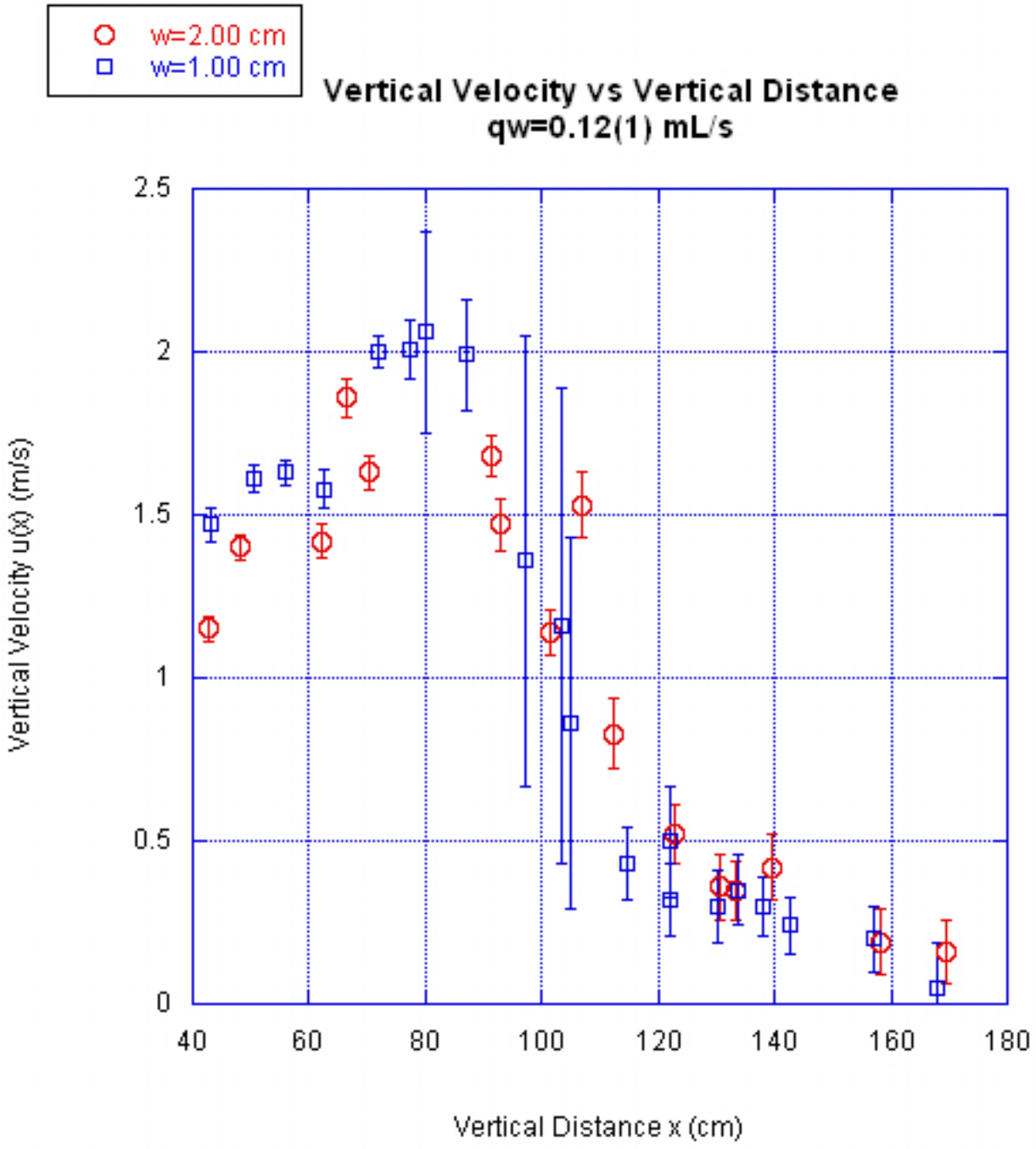

Figure 2.3: The velocity profile of a soap film at constant flux for two different film widths: w=1.00 cm and w=2.00 cm.

Reproduced from [5], Fig. 2.4 shows these measurements, indicating that the total length L palys a role in determining the location of the decrease in velocity, with the transition occurring at higher positions for shorter films.

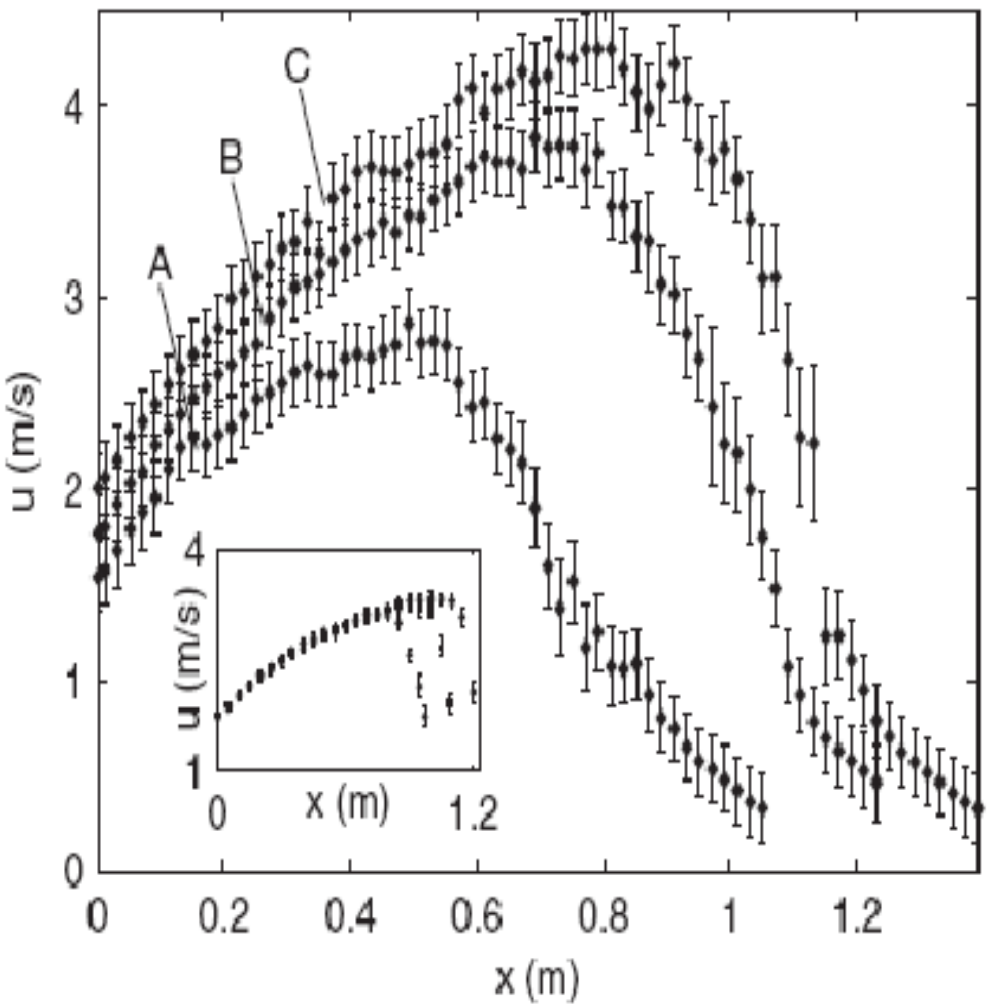

Figure 2.4: Plots of the mean velocity u vs x for three steady flows. The width =5.1 cm for all flows; both the length L and the flux per unit width q change from flow to flow. (A)L=1.05 m and $q = 3.8 \times 10^{-6}\ m^2/s$, (B)$L$=1.23 m and q=$4.9 \times 10^{-6}\ m^2/s$, (C)$L$=1.39 m and $q = 4.9x \times 10^{-6}\ m^2/s$. Inset: Plots of u vs x for three steady flows. w=5.1 cm and q= $5.7 \times 10^{-6}\ m^2/s$ for all flows; L changes from flow to flow. In this figure $x = 0$ where the film attains its maximum thickness after the expansion region l, not at the nozzle as in the previous graphs.

2.4.2 Thickness Profile

Under the assumptions of Sec. 2.2, $q = h(x)u(x)$, so the observed drop in velocity should correspond to a sudden increase in thicknesss. Using the interference photography and Fluorescein dye flourescence mentioned in Secs. 2.3.2 and 2.3.3, respectively, the thickness as a function of both the vertical distance x and the horizontal distance z was investigated. Interference fringes in the vertical region where the velocity abruptly decreased not only decreased in spacing but also deformed from a vertical orientation to a horizontal orientation, as can be seen in Figs. 2.5, 2.6, and 2.7(a), reproduced from [5]. This indicated an abrupt increase in thickness in the vertical direction. This conclusion was supported by the results of the Fluorescein dye fluorescence measurements (Sec. 2.3.3), which showed a rapid increase in the flourescent intensity (measured along the centerline of the film) in the same vertical region as the decrease in velocity and the change in the interference fringes. The exciting light source for the flourescence measurements was then placed atop a motorized stage and scanned horizontally (in the z direction) across the film at several vertical positions. The results, shown in Fig 2.7(b), confirmed our assumption that the thickness is approximately independent of z and provided further evidence of the increase in thickness.

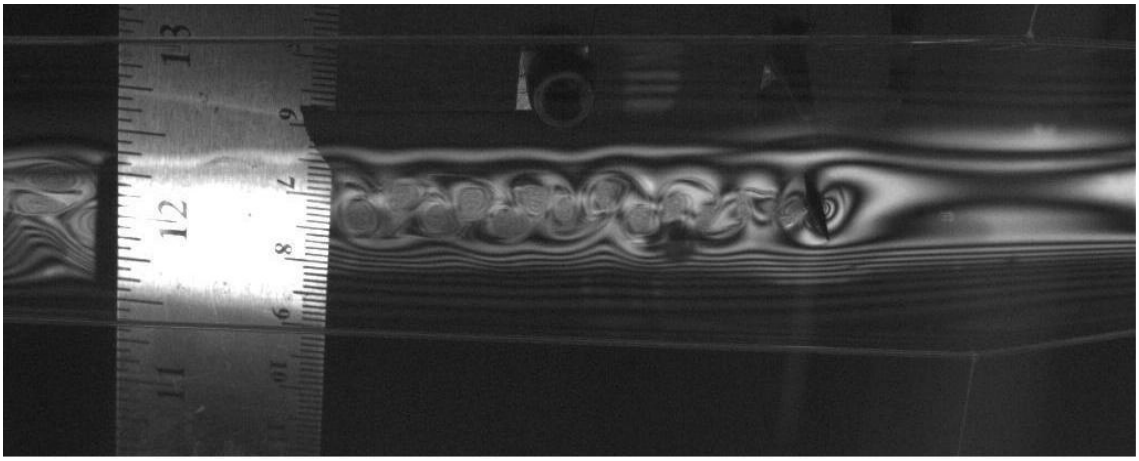

Figure 2.5: An interference photograph taken with a Phantom fast camera showing the interference fringes upstream of the thickness transition as well as the vortex wake generated by a conical rod inserted into the film. The ruler provides the length scale, and flow is from right to left.

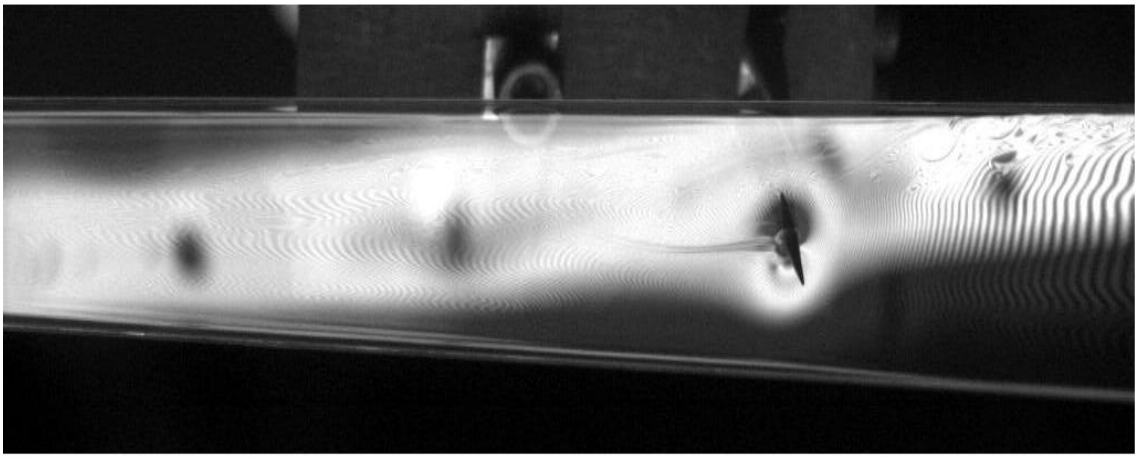

Figure 2.6: The interference fringes downstream of the thickness transition. Note how the wake of the conical rod is now a compressed line.

In addition to the measurements shown in Figs. 2.7(a) and 2.7(b), Tuan Tran of the University of Illinois Urbana-Champaign also measured a property of the soap film known as the Marangoni speed, U_M, which gives the velocity at which waves travel on the film surface due to the surface tension between the soap molecules. This was done by inserting a pin into the film both above and below the sudden tranisition in thickness. Measuring the angular spread of the wake disturbance upstream of the transition gives the Mach angle, which in this case was $\approx 50°$. The mean velocity at this point was measured to be $u = 1.84m/s$ using LDV. Since the propagation of the disturbance in the horizontal direction is solely due to the natural speed of the waves, $U_M = \sin 50° \times 1.83m/s = 1.4m/s$. The qualitative change between a broadly propagating disturbance upstream of the thickness transition and a thin wake downstream of the transition suggests that the velocity upstream of the transition is greater than that of surface waves in the film and the flow is thus supercritical, while the flow downstream of the transition is subcritical [5], as explained in Sec. 1.3.

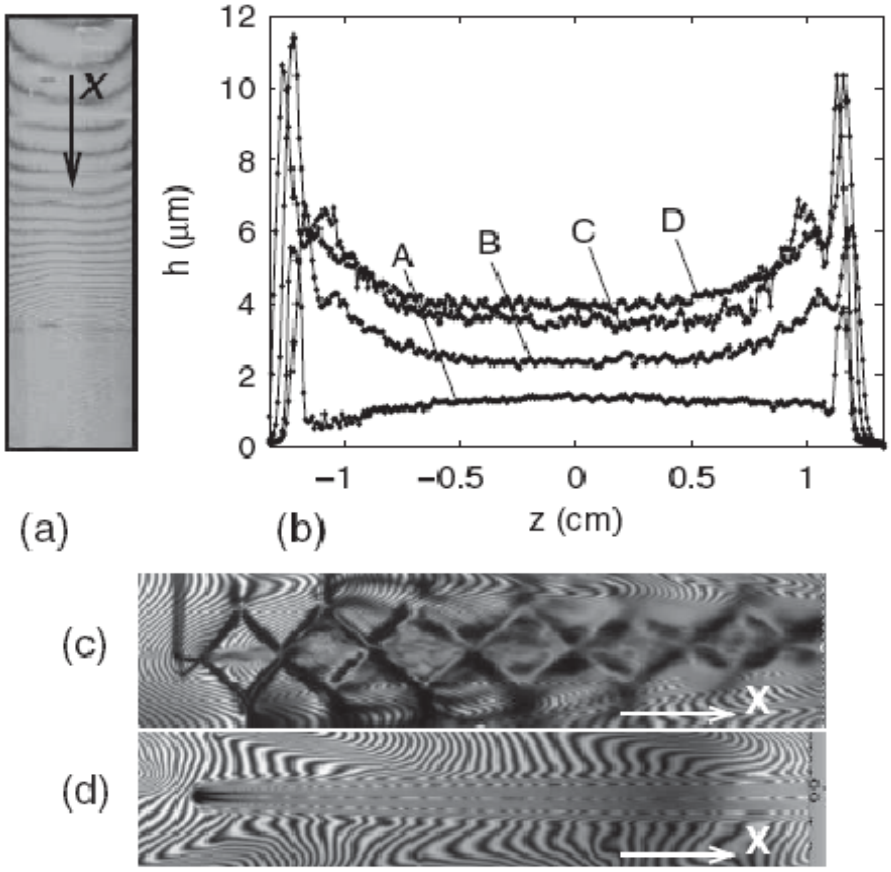

Figure 2.7: (a)Fringes over the part of a film where the velocity drops abruptly. (b)Plots of the thickness vs z along four cross sections of a flow of w=2.5 cm and L=1.2m. The cross sections are at x = 0.95 m (A), x = 1.04 m (B), xx = 1.05 m (C), and x = 1.07 m (D). The large peaks near the lateral edges are due to backscattering from the wires. Fringes at a piercing upstream (c) and downstream (d) of the drop in velocity; fields of view 5 cm × 1 cm.

2.4.3 Power Spectra of Velocity

As mentioned in Sec. 2.4.1, the rms velocity fluctuations were greater in the region of sudden change in film thickness (up to three times greater) than in the rest of the film, and Fig. 2.8 (reproduced from [5]) shows a graph of these fluctuations vs vertical distance to highlight this fact. Fourier analysis was performed on the square of the velocity data (since kinetic energy is dependent on the velocity *squared*) as measured along the vertical centerline of the film to provide the energy power spectrum, or the amount of energy associated with different length scales (see Sec. 1.2). The results of this analysis for a point above the transition, within the transition region, and below the transition are shown in the inset of Fig. 2.8 as points A, B, and C, respectively. The area under the energy spectrum corresponding to the thickness transition (B in the figure) is greater than the area under the spectra either above or below the transition, indicating a greater amount of energy associated with the velocity fluctuations and therefore more intense turbulent motion.

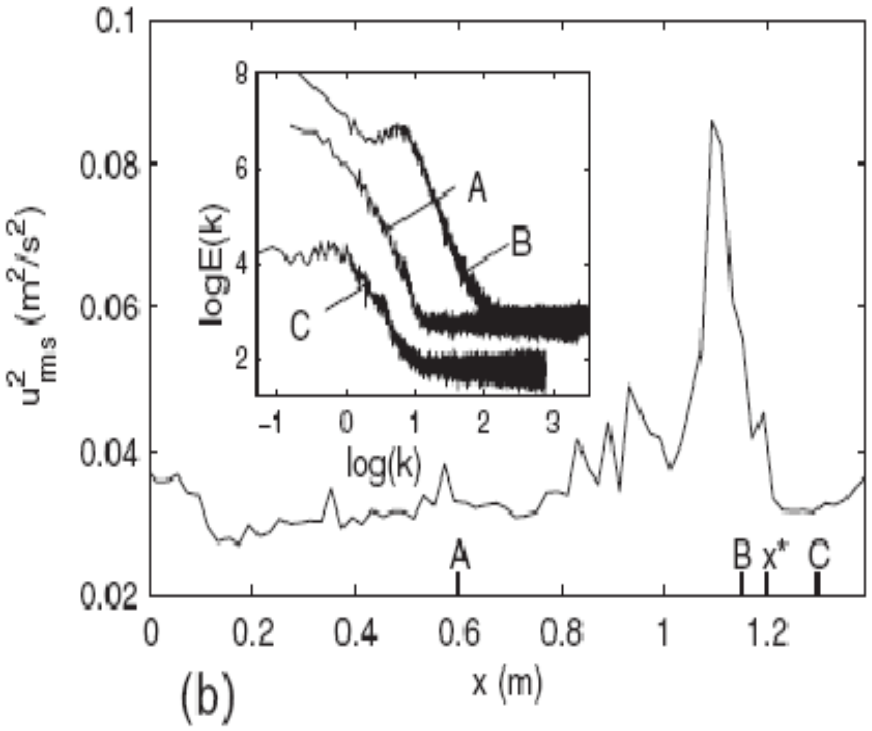

Figure 2.8: Plot of the experimental u^2_{rms} (an index of the energetic contents of the velocity fluctuations) vs x for the same flow. Inset: energy spectra at the center line of the same flow for the cross section as t $x = 0.60m$ (A), $x = 1.17m$(B), and $x = 1.30m$ (C). These are the cross sections marked A,B, and C in the larger graph. The spectra are log-log plots of the energy density E (m^3/s^2) vs wave number k ($1/m$).

3.0 THEORETICAL EXPLANATION OF RESULTS

As first proposed by Tuan Tran of the University of Illinois Urbana-Champaign, the experimentally observed change in thickness of the soap film is explained by the hydraulic jump phenomenon of free surface flows [5]. The sudden change in thickness over a short vertical distance is preceded and followed by regions where the thickness is comparatively constant, just as in the hydraulic jump of free surface flows. Hydraulic jumps are also associated with energy dissipation and an increase in turbulence over the region of the jump, while our data show increased velocity fluctuations and turbulent intensity in the transition region. When we recall that the jump also defines a transition between supercritical and subcritical flow and that such flows need not be defined by gravity waves but can also be defined with relation to the elastic waves of surface tension, it would seem that all the necessary ingredients for a hydrualic jump are present. Indeed, the difference in the propagation of disturbances arising from a pin (Sec. 2.4.2) placed in the film upstream and downstream of the transition bears witness to a supercritical to subcritical transition.

To quantify the location of the jump, several assumptions are made. Firstly, the velocity field of the soap film is taken to be in the steady state, which matches observations that the position of the thickness transition does not change with time. The frictional forces due to the wires are negligible compared to friction from the air next to the film [14], and

are ignored. Furthermore, the velocity, like the thickness, is assumed to be constant as a function of the z direction and to be non-zero only in the vertical direction. The momentum equation in the x direction is then written as

$$\rho h u u_x = 2\sigma_x + \rho g h - 2\tau_a \tag{3.1}$$

where σ is the surface tension, τ_a is the shear stress due to air friction, x is now measured from the first point when the film attains its maximum width (after the elongation section of length l), and we have switched the subscript notation to now mean the partial with respect to x, so in the case of the surface tension σ, $(\sigma)_x = \frac{d(\sigma)}{dx}$. The left-hand term is just the inertial term seen earlier in connection with the NSE, while the right-hand terms are the elastic force, the gravitational force, and the drag force of the ambient air, respectively. The friction term due to the surrounding air can be taken to be approximately the same as that of a rigid plate that moves through the air with a constant velocity u [14]. Thus, $\tau_a = 0.3\sqrt{\frac{\rho_a \mu_a u^3}{x+l}}$, with the density of air $\rho_a = 1.2\ kg/m^3$ and the viscosity of air $\mu_a = 1.7 \times 10^{-5}\ kg/ms$.

The force due to surface tension, $2\sigma_x$, is derived assuming that the film is in the Marangoni regime so that the surface deformations happened too quickly for any soap molecules within the bulk of the fluid to have time to diffuse into the surface. This can be justified by considering the length of time any fluid element will spend in the film. This time scale, call it τ_r, will be much greater than the time scale τ_d of any surface deformation since the surface deformation will occur at most over several centimeters, and thus the fluid element will pass through this distance in a time that is at least an order of magnitude less than the time for it to traverse the entire film. With a mean velocity on the order of 1 m/s and a film length on the order of 1 m, $\tau_r \approx 1$ s. But τ_D, the time scale associated

with diffusion of soap molecules, is also on the order of 1 s [12], and therefore the time scale for diffusion is much greater than the time scale of the thickness changes. Being in the Marangoni regime, the surface tension of the solution deviates from that of pure water by a factor $RT\Gamma$, where the R is the universal gas constant, T the temperature, and Γ the concentration of soap molecules at the surface. Furthermore, $\Gamma = \frac{(c-c_b)h}{2}$, where c is the concentration of soap molecules in the fluid, c_b is the concentration of soap molecules that remain in the bulk of the fluid, and h is the film thickness. Substitution of this expression for the surface tension and then differentiating yields

$$\sigma_x = -\rho U_M^2 h_x/2,$$

where U_m (the Marangoni speed) is defined as $RT(c - c_b)/\rho$.

Inserting this form for the surface tension into Eq. (3.1), remembering that $h = \frac{q}{u}$ and then rearranging terms leads to

$$u_x = u\frac{g - 2\tau_a u/\rho q}{u^2 - U_M^2} \tag{3.2}$$

Equation (3.2) leads to two specific solution regimes: when $u > U_M$, the flow is supercritical (since U_M is the velocity of elastic surface waves in the film), and $u_x > 0$; while when $u < U_M$, the flow is subcritical, and $u_x < 0$. These regimes are readily seen in the measurements that established that the flow was supercritical above the transition and subcritical below the transition (Fig. 2.7), and are consistent with the invariance of the upstream flow for a fixed q as the film length changes (see the inset of Fig. 2.4). Equation (3.1) has a discontinuity at $u = U_M$, and just as the hydraulic jump in a river was considered as a shock (discontinuity) in the shallow water equations (Sec. 1.3.1) by Lord Rayleigh, we can view the thickness

transition in the film as a shock in Eq. (3.2), a *Marangoni* shock since the restoring force is due to the Marangoni elasticity of the film.

In collaboration with Tran, Gioia, and Chrakraborty of the University of Illinois, supercritical and subcritical solutions to Eq. (3.2) were obtained through integration of this first order differential equation [5]. The supercritical solution is obtained by imposing the boundary condition $u(x = 0) = u_0$ where u_0 is the measured velocity where the wires attain their maximum width for any particular experiment. (Actually, $u(v)$ was used, where v=5.1 cm, so as to limit the end effects that the initial expansion of the wires from the single point of the nozzle would have on the solution. A similar procedure was used when taking the velocity at the bottom of the film.) The resulting function $u(x)$ should be a good fit to the experimental data upstream of the jump. Similary, the velocity at the end of the film, $u(x = L) = u_L$ can be imposed as a boundary condition to calculate $u(x)$ for the flow downstream of the jump. The other two parameters in Eq. (3.2), U_M and q, are adjusted to optimal values for each experimental data set, in the case of q, and for all the data sets as a whole, in the case of U_M. The results are shown in Fig. 3.1, reproduced from [5].

The transition from the supercritical to the subcritical solution is assumed to be instantaneous (the derivative of the velocity is infinite) at the point $x = x*$ where $x*$ is the point where $u = U_M$. This is inherent in modelling the hydraulic jump as a shock. However, the velocity profile of the actual jump is not discontinuous, and actually extends over a finite region Δx, as shown in Fig. 3.1. This naturally arises since the region of the hydraulic jump is turbulent, and our theory does not include turbulence and the accompanying energy dissipation (just as the original hydraulic jump theory of Lord Raylegih cannot resolve the jump structure). Future work could include applying the ideas of T. Bohr ([8]) to see if the

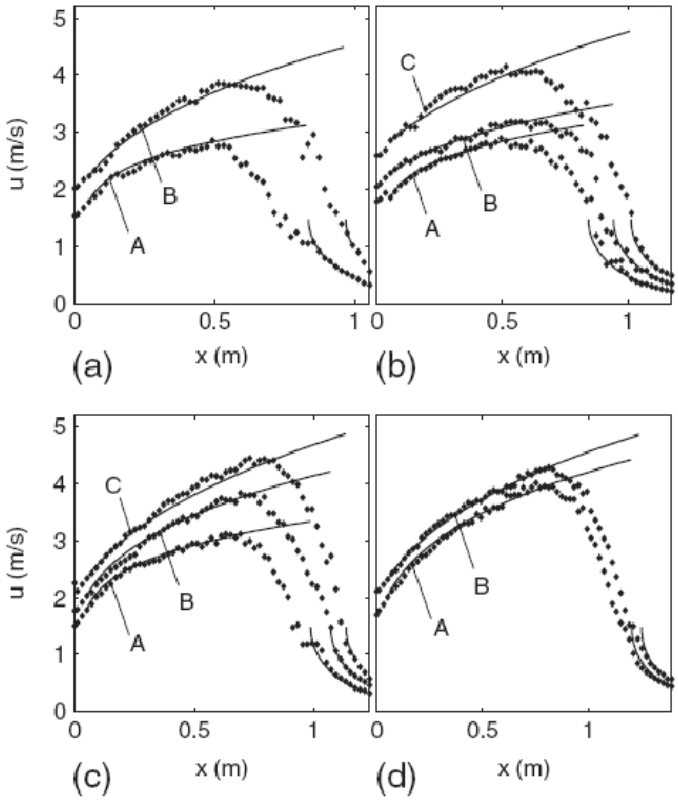

Figure 3.1: Plots of the computational $u(x)$ (lines) and experimental $u(x)$ (points) for ten different flows. The computations are for $U_M = 1.48$ m/s and the values of q indicated below (the experimental estimates for q are indicated in parentheses). w=5.1 cm for all flows. (a) Flows of length 1.05 m: (A) $q = 5.7 \times 10^{-6}\ m^2/s$ ($3.9 \times 10^{-6}\ m^2/s$), (B) $25 \times 10^{-6}\ m^2/s$ ($5.7 \times 10^{-6}\ m^2/s$); (b) flows of length 1.17 m: (A) $5.7 \times 10^{6}\ m^2/s$ ($5.1 \times 10^{-6}\ m^2/s$), (B) $7.4 \times 10^{6}\ m^2/s$ ($5.9 \times 10^{-6}\ m^2/s$), (C) $30 \times 10^{6}\ m^2/s$ ($7.5 \times 10^{-6}\ m^2/s$); (c) flows of length 1.23 m: (A) $6.1 \times 10^{6}\ m^2/s$ ($4.1 \times 10^{-6}\ m^2/s$), (B) $14 \times 10^{6}\ m^2/s$ ($5.3 \times 10^{-6}\ m^2/s$), (C) $31 \times 10^{6}\ m^2/s$ ($6.5 \times 10^{-6}\ m^2/s$); and (d) flows of length 1.39 m: (A) $16 \times 10^{6}\ m^2/s$ ($4.7 \times 10^{-6}\ m^2/s$), (B) $25 \times 10^{6}\ m^2/s$ ($6.3 \times 10^{-6}\ m^2/s$).

structure of the jump itself could be properly modeled.

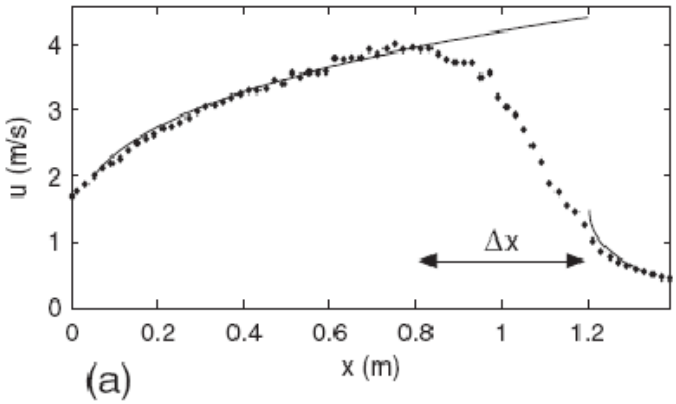

Figure 3.2: Plots of the computational u(x) (lines) and the experimental u(x) points for a representative flow. Δ x is the span of the shock.

4.0 CONCLUSION

A previously unobserved transition in the thickness of a gravity-driven soap film has been discovered and explained using the traditional inviscid theory of the hydraulic jump. The elastic forces associated surface tension are found to govern the formation of the jump, and the jump itself can be interpreted as a shock in the force equation governing the vertical component of velocity when the viscosity of the fluid is ignored. Experimentally, the jump has also been shown to produce a marked increase in turbulent fluctuations, resulting in an increase in energy dissipation within the film. The existence of this jump as well as the increased turbulent intensity merit special attention when studying 2D turbulence as the soap film has been a prominent model system in the field for several decades.

BIBLIOGRAPHY

[1] G.K. Batchelor. *An Introduction to Fluid Dynamics*. Cambridge University Press, New York, 2002.

[2] D. J. Tritton. *Physical Fluid Dynamics*. Clarendon Press, Oxford, 1988.

[3] Walter A. Strauss. *Partial Differential Equations: An Introduction*. John Wiley and Sons, Inc., USA, 1992.

[4] Uriel Frisch. *Turbulence: The Legacy of AN Kolmogorov*. Cambridge University Press, New York, 2004.

[5] T. Tran, P. Chakraborty, G. Gioia, S. Steers, and W. Goldburg. Marangoni shocks in unobstructed soap film flows. *Physical Review Letters*, 103:104501, 2009.

[6] V.T. Chow. *Open Channel Hyrdraulics*. McGraw-Hill Book Company, Inc., New York, 1959.

[7] Lord Rayleigh. On the theory of long waves and bores. *Proc. R. Soc. London A*, 90:324, 1914.

[8] T. Bohr, V. Putkaradze, and S. Watanabe. Averaging theory for the structure of hydraulic jumps and separation in laminar free-surface flows. *Physical Review Letters*, 79:1038–1041, 1997.

[9] James Lighthill. *Waves in Fluids*. Cambridge University Press, New York, 2005.

[10] D. Randall. The shallow water equations. Selected paper (2006), available at kiwi.atmos.colostate.edu/group/dave/pdf/ShallowWater.pdf.

[11] H. Schlichting and K. Gersten. *Boundary Layer Theory.* Springer-Verlag, New York, 2003.

[12] Y. Couder, J.M. Chomaz, and M. Rabaud. On the hydrodynamics of soap films. *Physica (Amsterdam)*, 37D:384–405, 1989.

[13] M. A. Rutgers, X. L. Wu, and W. B. Daniel. Conducting fluid dynamics experiments with vertically falling soap films. *Review of Scientific Instruments*, 72:3025–3037, 2001.

[14] M. A. Rutgers et. al. Two-dimensional velocity profiles and laminar boundary layers in flowing soap films. *Phyiscs of Fluids*, 8:2847–2854, 1996.